Investigating the role of tumour cell derived iNOS on tumour growth and vasculature *in vivo* using a tetracycline regulated expression system

Journal:	*International Journal of Cancer*
Manuscript ID	IJC-15-1799.R1
Wiley - Manuscript type:	Research Article
Date Submitted by the Author:	n/a
Complete List of Authors:	Papaevangelou, Efthymia; The Insitute of Cancer Research, Radiotherapy & Imaging Whitley, Guy; St. George's University of London, Cardiovascular and Cell Sciences Research Institute Johnstone, Alan; St. George's University of London, Cardiovascular and Cell Sciences Research Institute Robinson, Simon; The Insitute of Cancer Research, Radiotherapy & Imaging Howe, Franklyn; St. George's University of London, Cardiovascular and Cell Sciences Research Institute
Key Words:	nitric oxide , nitric oxide synthase, inducible expression , MRI, tumour vessel maturation

Investigating the role of tumour cell derived iNOS on tumour growth and vasculature *in vivo* using a tetracycline regulated expression system

Running title: Tumour cell derived iNOS and vasculature

Efthymia Papaevangelou[1*], Guy S. Whitley[1], Alan P. Johnstone[1], Simon P. Robinson[2], Franklyn A. Howe[1]

[1]Cardiovascular and Cell Sciences Research Institute, St. George's, University of London, Cranmer Terrace, London SW17 0RE, UK.

[2]Division of Radiotherapy and Imaging, The Institute of Cancer Research, 15 Cotswold Road, Belmont, Sutton, Surrey SM2 5NG, UK.

*Correspondence to: Efthymia Papaevangelou, Cancer Research UK Cancer Imaging Centre, Division of Radiotherapy and Imaging, The Institute of Cancer Research, 15 Cotswold Road, Belmont, Sutton, Surrey SM2 5NG, United Kingdom, Tel.: 020-8722-4321, Fax: 020-8661-0846, E-mail: Efthymia.Papaevangelou@icr.ac.uk

Keywords: nitric oxide, nitric oxide synthase, inducible expression, MRI, tumour vessel maturation

Article category: Molecular Cancer Biology

Novelty and impact: The role of nitric oxide in cancer is contentious and has been attributed both tumour inhibitory and promoting properties. We show that tumour-derived inducible nitric oxide synthase is an important mediator of tumour growth and vessel maturation, hence a promising therapeutic target. Moreover, the combination of intrinsic and extrinsic susceptibility magnetic resonance imaging provides a non-invasive biomarker of tumour vascular function, hence may aid assessment of response to anti-vascular therapies, such as iNOS inhibitors.

Abstract

Nitric oxide (NO) is a free radical signalling molecule involved in various physiological and pathological processes, including cancer. Both tumouricidal and tumour promoting effects have been attributed to NO, making its role in cancer biology controversial and unclear. To investigate the specific role of tumour-derived NO in vascular development, C6 glioma cells were genetically modified to include a doxycycline regulated gene expression system that controls the expression of an antisense RNA to inducible nitric oxide synthase (iNOS) in order to manipulate endogenous iNOS expression. Xenografts of these cells were propagated in the presence or absence of doxycycline. Susceptibility magnetic resonance imaging (MRI), initially with a carbogen (95% O_2 / 5% CO_2) breathing challenge and subsequently an intravascular blood pool contrast agent, was used to assess haemodynamic vasculature (ΔR_2*) and fractional blood volume (fBV), and correlated with histopathological assessment of tumour vascular density, maturation and function. Inhibition of NO production in C6 gliomas led to significant growth delay and inhibition of vessel maturation. Parametric fBV maps were used to identify vascularised regions, from which the carbogen-induced ΔR_2* was measured and found to be positively correlated with vessel maturation, quantified *ex vivo* using fluorescence microscopy for endothelial and perivascular cell staining. These data suggest that tumour-derived iNOS is an important mediator of tumour growth and vessel maturation, hence a promising target for anti-vascular cancer therapies. The combination of ΔR_2* response to carbogen and fBV MRI can provide a marker of tumour vessel maturation that could be applied to non-invasively monitor treatment response to iNOS inhibitors.

Introduction

Nitric oxide (NO) is an important pleiotropic signalling molecule involved in physiological and pathophysiological processes, and has been detected in a variety of human tumours, including colon, breast, prostate, and brain.[1, 2] The effect of NO in tumours depends upon the exposure to NO in terms of duration and concentration, the intrinsic sensitivity of cells to NO, and the expression, activity and temporal distribution of the three nitric oxide synthases (NOS): neuronal (nNOS or NOS1), inducible (iNOS or NOS2), and endothelial (eNOS or NOS3) that catalyse the synthesis of NO from L-arginine.[2] Tumour cells express iNOS and in some cases nNOS and eNOS, tumour-associated immune cells and stromal fibroblasts express iNOS, and vascular endothelial cells mainly express eNOS.[3]

The effect of NO in cancer has been the cause of intense debate due to its dichotomous nature, with studies indicating that NO has both tumour inhibitory and promoting properties.[4, 5] iNOS has also been implicated in tumour progression and angiogenesis. In human cancers, such as colon adenocarcinomas,[6] and central nervous system cancers,[7] increased iNOS expression and activity was positively correlated with vascularisation and higher tumour grade. In human gliomas, high iNOS expression was inversely correlated with patient survival irrespective of the tumour grade, suggesting that iNOS expression is a negative prognostic factor for glioma patients.[8] Overexpression of iNOS in human colon adenocarcinoma xenografts increased tumour growth and angiogenesis,[9, 10] whereas iNOS overexpression in melanoma and prostate tumours induced apoptosis and delayed tumour growth.[11, 12]

Manipulation of NO can be achieved pharmacologically with NO donors[13] or NOS inhibitors,[14] or genetically such as in iNOS knockout mice.[15] NO inhibition by selective or non-selective NOS inhibitors can reduce tumour growth and have anti-angiogenic effects.[16-18] Moreover, the NOS inhibitor N-nitro-L-arginine (L-NNA) elicited tumour anti-vascular effects in a phase I clinical trial.[19] However, pharmacological NOS inhibition could lead to

adverse systemic effects, including hypertension, sinus bradycardia and palpitation.[19] Studies with NO donors suggest a concentration-dependent role of NO, whereby low concentrations of NO donors inhibit tumour growth and angiogenesis, whereas high concentrations reduce the anti-tumour response due to interference with the host physiology and can affect not only tumour- but also stromal-derived NO.[13] A more refined approach is afforded by genetic manipulation of tumour cells in which iNOS is either overexpressed[10, 20] or suppressed,[21, 22] enabling the specific investigation of the effects of tumour cell-derived NO.

In the present study, a novel doxycycline inducible iNOS expression system was engineered to robustly interrogate the role of exclusively tumour-derived iNOS on tumour growth and vascular development in subcutaneous C6 gliomas using *in vivo* MRI and *ex vivo* histopathological analysis.

Materials and Methods

Cell culture

C6 rat glioma cells (European Collection of Cell Cultures, Salisbury, UK) were maintained in Nutrient Ham's F-10 (Sigma-Aldrich, Dorset, UK) medium supplemented with 2 mM L-glutamine, 100 U/ml penicillin, 0.2 mg/ml streptomycin and 10% (v/v) fetal bovine serum.

To achieve intrinsic, inducible inhibition of tumour-derived iNOS, C6 cells were engineered to include an antisense iNOS cDNA sequence combined with a tetracycline inducible system (pTet Off), where gene expression is controlled by doxycycline, the water soluble derivative of tetracycline (Supplementary Methods). Stably transfected cells (designated C6 pTet-off asiNOS) were grown in the presence or absence of 2 μg/ml doxycycline.

Nitric oxide production

Cells were stimulated with cytokines (10 ng/ ml TNF-α, 1000 U/ml IFN-γ) and 5μg/ml LPS. Nitrite production provided a proxy measure of NO synthesis determined using the Griess reaction.[23] To detect total NO in tumour homogenates, nitrate was reduced to nitrite using vanadium chloride and the total nitrate plus nitrite (NOx) determined using the Griess reaction.[24]

Western blot analysis

The protein concentration of cell lysates or tumour homogenates was determined using the Bradford assay[25] and equal amounts of protein were analysed by SDS–PAGE. iNOS expression was detected using a rabbit polyclonal anti-mouse iNOS antibody (M-19) (sc-650, Santa Cruz, Heidelberg, Germany), a goat anti-rabbit horseradish peroxidase (HRP) (Dako Ltd., Cambridgeshire, UK), and an Immobilon Western Chemiluminescent HRP

substrate (GE Healthcare, Chalfont St. Giles, UK). A polyclonal anti-α-actin antibody (Sigma-Aldrich) was used to verify equal protein loading.

Animals and Tumours

Experiments were performed in accordance with the UK Home Office Scientific Procedures Act 1986. Female (7 - 8 weeks old) NCr nude mice were injected subcutaneously in the flanks with 2 x 10^6 cells in 0.1 ml phosphate-buffered saline (PBS). Tumour size was measured using callipers and tumour volume calculated assuming an ellipsoid shape, using: $(\pi/6) \times L \times W \times D$, where L, W and D are the largest orthogonal dimensions of the ellipsoid. Animals were given drinking water containing 5% (w/v) sucrose with or without 0.2 mg/ml doxycycline. Doxycycline administration started five days prior to tumour cells injection and was maintained until the end of the experiment. The drinking water containing sucrose ± doxycycline was changed every other day. Henceforth, tumours grown without doxycycline will be referred to as NO^- tumours and tumours grown with doxycycline as NO^+ tumours.

Magnetic resonance imaging

Mice bearing size-matched tumours grown in the presence or absence of doxycycline were anaesthetised with a 10 ml/kg intraperitoneal injection of Hypnorm (0.315 mg/ml fentanyl citrate plus 10 mg/ml fluanisone; Janssen Pharmaceutical, Wantage, UK), Hypnovel (5 mg/ml midazolam; Roche, West Sussex, UK) and water (1:1:2). A lateral tail vein was then cannulated with a heparinised 27-gauge butterfly catheter for contrast agent administration during MRI. The mouse was positioned so the tumour hung within a three-turn 25 mm diameter surface coil for MRI using a 4.7 T Varian Unity INOVA horizontal small-bore imaging system. A nose cone was positioned for breathing gas delivery, and heated air blown through the magnet bore used to maintain the mouse core temperature at 37°C.

Blood oxygen saturation was monitored using a MouseOx Pulse Oximeter (Braintree Scientific, Massachusetts, US).

T_2-weighted spin echo images were acquired from seven axial 1 mm thick slices positioned across the whole tumour, using a repetition time (TR) of 1500 ms, an echo time (TE) of 30 ms, and a 128 x 128 matrix over a 2.56 cm field of view. Susceptibility MRI was used to quantify changes in the tumour MRI transverse relaxation rate R_2* (s^{-1}) caused by perturbations in the paramagnetic deoxyhaemoglobin (dHb) content in the blood vessels. Carbogen (95% O_2 / 5% CO_2) breathing, a hypercapnic hyperoxia challenge, was used to increase blood oxygenation, and to probe for localised vascular smooth muscle dilation via blood flow induced oxygenation changes, and hence to assess vessel function and maturation.[26-28] Multi-gradient echo (MGRE) images were acquired from seven slices with TR of 450 ms, TE of 7 to 56 ms, an echo spacing of 7 ms and flip angle (α) of 45°. MGRE images were acquired during air and then, following a 5 minute transition period, during carbogen breathing.

Air breathing was then resumed and once the mouse blood oxygen saturation had recovered to initial air-breathing levels, tumour fractional blood volume (fBV, %) was quantified by susceptibility contrast MRI, utilising ultrasmall superparamagnetic iron oxide (USPIO) particles as a blood pool contrast agent. USPIO particles create magnetic susceptibility variations close to blood vessels, increasing R_2* of water in the surrounding tissue. Their long intravascular half-life enables steady-state measurements of tumour R_2* to be made to determine fBV.[29] MGRE images were acquired prior to and 5 minutes after intravenous injection of 5.2 mgFe/kg of the USPIO contrast agent ferumoxtran (Guerbet S.A., Villepinte, France).

MRI data analysis

R_2* maps were calculated on a voxel-by-voxel basis from MGRE image data using ImageJ and Matlab. Average apparent R_2* relaxation rates were calculated for each slice for a region of

interest (ROI), defined from the associated T_2-weighted image, encompassing the whole tumour but excluding the surrounding skin and muscle. Carbogen-induced changes in R_2^* ($\Delta R_2^*_{CB} = R_2^*_{carbogen} - R_2^*_{air}$) were determined over the whole tumour. Tumour fBV was determined over the same ROI from the increase in R_2^* ($\Delta R_2^*_{USPIO} = R_2^*_{post\text{-}USPIO} - R_2^*_{pre\text{-}USPIO}$) caused by the USPIO particles.[29]

To reduce contributions from noise and from averaging over necrotic and poorly perfused tumour regions in the global measurement of carbogen-induced ΔR_2^*, a retrospective analysis of the intrinsic susceptibility data was performed using the calculated fBV. The median fBV from all tumours was applied as a threshold to define vascularised regions in the $\Delta R_2^*_{CB}$ maps, and hence measure the carbogen-induced ΔR_2^* that relates to vascular tumour tissue.

Immunohistochemistry and fluorescence microscopy

Immediately following MRI, mice were administered intraperitoneally with 60 mg/kg of the hypoxia marker pimonidazole hydrochloride (Hypoxyprobe, Burlington, MA, USA) in PBS. After 45 min mice were injected intravenously through a lateral tail vein with 15 mg/kg of the perfusion marker Hoechst 33342 (Sigma-Aldrich, Dorset, UK) in PBS. Tumours were excised after 1 min and snap-frozen. For each tumour, three acetone-fixed cryosections (10 µm) were visualized for Hoechst 33342 uptake by fluorescence microscopy at 365 nm using a motorized scanning stage (Prior Scientific Instruments, Cambridge, UK) attached to a BX51 microscope (Olympus Optical, London, UK) driven by CellP (Soft Imaging System, Munster, Germany) to record composite digital images of whole tumour sections. The same sections were then processed for the formation of pimonidazole adducts, using Hypoxyprobe-1 plus FITC-conjugated mouse monoclonal antibody (1/1000) and recorded at 450-490 nm using the same stage coordinates. To assess endothelial and perivascular cell content, additional sections were stained with rat monoclonal anti-mouse CD31 antibody [MEC 7.46] (1/50, ab7388, Abcam, Cambridge, UK), biotinylated goat anti-mouse

immunoglobulin (IgG) (1/300, Vector Laboratories, Peterborough, UK) and Fluorescein Avidin D (1/250, Vector Laboratories), and subsequently, with rabbit polyclonal antibody against smooth muscle actin (α-SMA, 1/200, ab5694, Abcam) and Alexa-Fluor 546 goat anti-rabbit secondary antibody (1/1000, Invitrogen, Paisley, UK). Non-immune mouse and rabbit IgG antibodies were used in the same concentration with CD31 and α-SMA antibodies respectively, to be used as negative isotype controls. Fluorescein Avidin D was detected at 495-515 nm and Alexa-Fluor 546 at 556-573 nm and composite images were recorded.

Post-processing was performed on composite digital images using CellP or ImageJ software [30]. ROIs encompassing the whole tumour sections were defined and fluorescent particles detected above a constant across all sections colour threshold, which was higher than background fluorescence as defined from the negative control stained tumour sections. The area of the tumour section with Hoechst 33342, pimonidazole adduct, CD31 or α-SMA fluorescence was determined and expressed as a percentage of the whole tumour section, and for each tumour the average across three slices was determined.

Haematoxylin and eosin staining

Frozen tumour sections were stained with haematoxylin and eosin (H&E) and visualized under light microscopy using the same system as for the detection of fluorescence. Composite images of whole tumour sections were recorded and ROIs drawn around all necrotic foci using ImageJ. For each tumour, necrosis was expressed as a percentage averaged across three slices.

VEGF ELISA

Culture medium was collected when confluent from 3cm dishes 72 h after seeding and analysed for VEGF expression using a rat VEGF ELISA kit (PeproTech, London, UK) according to manufacturer's instructions. VEGF expression was also measured in tumour

homogenates. Values were normalized to the protein concentration of cells or tumours, determined using the Bradford assay.[25]

Statistical analysis

Results are presented as mean ± 1 standard error of the mean (SEM) with significance testing at a 5% confidence level. Student's unpaired *t*-test was used to compare two groups, whereas repeated measures ANOVA with Bonferroni's Multiple Comparison post-test was used to compare multiple groups.

Results

Generation of a switchable system for iNOS expression in C6 glioma cells

The basal expression of iNOS and the synthesis of NO by the C6 pTet-off asiNOS cells in the presence or absence of doxycycline were barely detectable. Stimulation of C6 pTet-off asiNOS with cytokines and LPS for two days in the presence of doxycycline (designated NO^+) resulted in the increased expression of iNOS and a two-fold increase in the production of NO as determined by nitrite. In the absence of doxycycline (designated NO^-), an antisense iNOS RNA was expressed, which blocked the stimulated expression of iNOS and inhibited the production of NO (Figure 1). Reduced iNOS expression did not affect the growth properties of cells *in vitro*. Growth rates of the cells, determined by measuring cell proliferation and death over 5 days, were the same in the presence or absence of doxycycline (Supplementary Figure 1).

In vivo investigation of NO manipulation on tumour growth

Endogenous iNOS protein was expressed in C6 pTet-off asiNOS tumours grown in animals drinking doxycycline. However, iNOS expression was limited in tumours grown without doxycycline (Figure 2A). Decreased iNOS expression led to a reduction in NO production. Nitrite production was similar in tumours grown in the presence or absence of doxycycline (data not shown). However, nitrite is an unstable product and can be further oxidized to nitrate. NOx (nitrite plus nitrate) production was reduced (3.5-fold) in NO^- tumours compared with NO^+ tumours (Figure 2B). NO^- tumours had significantly reduced growth rates compared with the NO^+ tumours. The mean tumour volume at 46 days post-inoculation was approximately half in the absence of NO compared with its presence (Figure 2C).

Effects of NO down-regulation on tumour vascular development

Mice bearing size-matched tumours were selected for MRI. There was no significant difference in mean tumour volume between NO^+ (632 ± 192 mm^3) and NO^- (554 ± 65 mm^3) cohorts at the time of imaging, which was 46 ± 4 days (post-inoculation) for the NO^+ and 54 ± 1 days for the NO^- tumours. Representative T_2-weighted images and parametric maps of baseline R_2*, fBV and carbogen-induced ΔR_2* from both tumours cohorts are shown in Figure 3A. No significant differences were found between the R_2* determined during air breathing prior to carbogen challenge (R_2*_{air}), and those prior to administration of USPIO particles ($R_2*_{pre\text{-}USPIO}$). All mice responded to carbogen breathing with an increase in blood oxygen saturation of 3.9 ± 2.5% in the NO^- group and 5.2 ± 1.8% in the NO^+ group. Carbogen induced a negligible change in R_2* averaged over the whole tumour in both cohorts. NO^- tumours exhibited a significantly higher overall fBV compared with the NO^+ tumours (Figure 3B). For tumour regions selected with vascular volume greater than the overall median, there was no difference in fBV between the two cohorts (Figure 3C). However, for these regions the intrinsic susceptibility MRI data revealed a significantly greater reduction in R_2* with carbogen breathing in NO^+ compared with NO^-tumours (Figure 3D). Thus, a smaller ΔR_2*_{CB} response was observed in the NO^- tumours in regions with similar fBV to NO^+ tumours.

Representative histological images from both tumour groups are shown in Figure 4. The Hoechst 33342-perfused area was significantly higher in the NO^- tumours compared with NO^+ tumours (Figure 5A). The degree of hypoxia was similar between the two groups (Figure 5B). The extent of necrosis was significantly higher in the NO^+ compared with the NO^- tumours (Figure 4B and 5C). The endothelial cell content of NO^- tumours was significantly higher than in tumours with NO (Figure 5D). Conversely, the perivascular cell content was almost double in NO^+ compared with NO^- tumours (Figure 5E). The fraction of mature vessels, quantified using the ratio of α-SMA stained area versus the CD31 stained area, was significantly higher in NO^+ compared with NO^- tumours (Figure 5F).

Effect of iNOS down-regulation on VEGF production

In stimulated cells, the presence of NO led to a 3-fold increase in VEGF production compared with the absence of NO (Figure 6A). In the absence of NO, stimulation did not affect VEGF synthesis. Moreover, when NO was produced, stimulation increased VEGF production by 1.7-fold. In tumour homogenates, the decreased NO production did not modify VEGF expression (Figure 6B).

Discussion

In the present study, a novel tetracycline inducible iNOS expression system was generated in order to exclusively investigate the role of tumour cell-derived iNOS on tumour growth and angiogenesis. In this system, the expression of antisense iNOS by the tumour cells was repressed when doxycycline was added to the cell culture medium or to the drinking water of tumour-bearing animals, and hence the expression of iNOS was maintained at basal endogenous levels. In the absence of doxycycline, an antisense iNOS RNA was expressed, which in turn blocked the expression tumour cell-derived iNOS. Some expression was still evident in the micro-environment of these tumours, presumably arising from accessory cells from the host such as macrophages, fibroblasts and endothelial cells, known additional sources of iNOS.[31] MRI was performed *in vivo* to non-invasively assess tumour vascular function, and compared with *ex vivo* histopathology.

In designing this Tet-inducible tumour model, we chose an antisense iNOS approach rather than an overexpression model, because iNOS overexpression could result in non-physiological concentrations of NO, which in turn could lead to non-specific effects on both tumour and host. For example, high NO concentration could result in accumulation of cytotoxic molecules, such as superoxide, hydrogen peroxide, peroxynitrite, and hydrogen cyanide.[32, 33] Moreover, high concentrations of NO can lead to vascular 'steal' effects, which involve the redistribution of blood away from the tumour, as a result of NO-mediated systemic vasodilation.[34, 35] By using an antisense iNOS approach rather than an overexpression genetically modified model, non-specific effects on both tumour and host can be avoided. The Tet Off regulation system offers the advantage of using the transfected cells themselves as internal controls, as the gene of interest in these cells is silenced in the presence of doxycycline.[36] Constitutive expressing systems in which the gene of interest is always expressed demand the use of mock transfected cells as control, which may lead to clonal variation complicating the results.[37]

In our C6 inducible glioma model, suppression of tumour cell-derived NO reduced the tumour growth rate. Pharmacological iNOS inhibitors, such as 1400W and BYK191023, have been shown to reduce the progression of subcutaneous and intracranial human glioma xenografts in mice,[8] and systemic iNOS inhibition with L-NAME reduced growth and induced significant necrosis in orthotopic C6 rat gliomas.[38] Similarly, C6 tumours constitutively expressing antisense iNOS grew significantly slower compared with wild type.[22] Additionally, constitutive expression of iNOS in human DLD1 colon cancer xenografts resulted in increased tumour growth.[10, 20] Our study suggests that differences in tumour growth between wild type and genetically engineered iNOS knockout C6 tumours reported in previous studies[21, 22] are specifically due to the effects of tumour-derived NO on tumour growth, and not a consequence of clonal variation on the growth rates between wild type and transfected cells.

The mechanism(s) by which the expression of iNOS in tumour cells promotes growth is still unclear; increased proliferation, enhanced migration and invasion, increased angiogenesis due to VEGF upregulation.[6, 10, 39] In the present study, the reduced growth observed in NO-deficient tumours was due neither to changes in the cell's inherent ability to divide (no difference in *in vitro* growth) nor reduced VEGF production. Tumour VEGF expression was similar for NO^- and NO^+ tumours. Similarly, reduced iNOS expression in C6 cells constitutively expressing antisense iNOS did not correlate with decreased VEGF expression compared with wild type tumours.[22] Since the confounding factor of clonal variability has been avoided, our results suggests that in C6 tumours VEGF production is not reliant on the production of NO and that NO is involved in VEGF-independent mechanisms enhancing tumour growth.

iNOS activity could promote tumour growth by maintaining tumour blood vessel tone and function.[2] Cullis *et al* showed that iNOS overexpression increases tumour growth, functionally perfused vasculature and angiogenesis.[9] Whittle *et al* reported that NOS was

expressed in orthotopic C6 rat brain tumours, and that NO-mediated mechanisms contributed to regulation of tumour blood flow and vessel dilatation.[40] In the same model, systemic NOS inhibition with L-NAME caused a greater reduction in tumour blood flow compared with normal brain. In a similar C6 model, NOS was found to regulate tumour blood flow [41]. In a previous study of subcutaneous C6 tumours with limited iNOS expression there was reduced tumour growth due to a dysfunctional vascular network and impaired tumour perfusion.[22] In our C6 inducible model, NO^- tumours appeared to have a better vascular supply, as indicated by the significantly higher fBV, increased perfusion and higher microvessel density, compared with NO^+ tumours. However, NO^+ tumours were more necrotic compared with NO^- tumours; hence, the fraction of viable tissue was higher in the latter. This is in agreement with a study in GH3 prolactinomas, which showed a correlation between low fBV and increased necrosis, as necrotic areas are devoid of blood vessels.[42] In contrast, in the study by Kostourou *et al*, NO-deficient tumours, despite their slower growth rate, had lower fBV and were more necrotic with less viable tissue compared with wild type C6 tumours, while vessel density was similar.[22] The present study, by using the Tet Off inducible system to manipulate NO production in a single cell line, overcomes the effects of clonal variation on tumour vascular characteristics experienced in previous studies, hence more accurately provides a measure of how endogenous tumour-derived NO affects growth and vascular development. Increased necrosis in our faster-growing NO^+ tumours is consistent with them outgrowing their blood supply and rate of new vessel development, leading to nutrient and oxygen deprivation and ultimately cell death.

Tumour vascular maturation, manifested by perivascular cell recruitment, can be detected by comparing susceptibility MRI in response to hypercapnic gas challenges with carbogen and with air-CO_2 (95% air and 5% CO_2); which utilizes the ability of mature vessels to dilate in response to elevated levels of CO_2.[43] In the present study we have used susceptibility MRI in response to hypercapnic hyperoxia to assess CO_2-reactivity in well vascularised regions determined by susceptibility MRI with a blood pool contrast agent. Combining spatial

information from both the carbogen breathing response and the measurement of vascular volume provides a better assessment of vascular characteristics than do the separate measurements.[44, 45] We have now demonstrated that in regions of similar vascular volume, the NO^+ tumours had a greater ΔR_2* response to carbogen compared to the NO^- tumours, which was correlated with a higher perivascular cell content and fraction of mature vessels. Thus, our study suggests a more mature and functional vascularity in the presence of NO and highlights the importance of tumour-derived NO in vessel maturation. Studies have shown that NO produced by eNOS in vascular endothelial cells plays a crucial role in vessel maturation by promoting perivascular cell recruitment. In B16 murine melanomas, reduction of NOS expression via NO blockade resulted in decreased perivascular cell coverage.[46] Ischaemic limbs of $eNOS^{-/-}$ mice also presented reduced perivascular cell coverage.[47] However, in our study the effect of NO on vessel maturation is mediated by iNOS, rather than eNOS, as NO production was modulated by specifically regulating iNOS expression.

In conclusion, NO derived from iNOS expressed by tumour cells plays a crucial role in the development of our C6 iNOS-inducible tumours, as not only does it promote tumour growth, but it is also involved in the recruitment of perivascular cells during the maturation of the neovasculature at the later stages of angiogenesis. These findings reinforce the concept of iNOS as a target for anti-vascular therapy of cancer. Our study also highlights the ability of susceptibility MRI to non-invasively investigate tumour vasculature and detect differences in tumour vascular phenotype induced by NO, indicating that a combined fBV and carbogen-induced ΔR_2* analysis may provide a non-invasive biomarker of tumour vascular maturation.

Acknowledgements

This work was supported by a Medical Research Council (MRC) and St. George's Hospital Medical School PhD studentship awarded to EP, the Association for International Cancer Research (AICR) (Grant No. 09-0310) and the Biotechnology and Biological Sciences Research Council (Grant No. S20430). The authors would like to thank Prof Judith Cartwright for providing the original clone for the murine antisense-iNOS, and Glyn Fisher and his staff for animal care.

References

1. Janakiram NB, Rao CV. iNOS-selective inhibitors for cancer prevention: promise and progress. *Future medicinal chemistry* 2012;**4**: 2193-204.

2. D'Amato RJ, Loughnan MS, Flynn E, Folkman J. Thalidomide is an inhibitor of angiogenesis. *Proceedings of the National Academy of Sciences of the United States of America* 1994;**91**: 4082-5.

3. Fukumura D, Kashiwagi S, Jain RK. The role of nitric oxide in tumour progression. *Nature reviews Cancer* 2006;**6**: 521-34.

4. Lechner M, Lirk P, Rieder J. Inducible nitric oxide synthase (iNOS) in tumor biology: The two sides of the same coin. *Seminars in Cancer Biology* 2005;**15**: 277-89.

5. Lala PK, Chakraborty C. Role of nitric oxide in carcinogenesis and tumour progression. *The lancet oncology* 2001;**2**: 149-56.

6. Ambs S, Merriam WG, Bennett WP, Felley-Bosco E, Ogunfusika MO, Oser SM, Klein S, Shields PG, Billiar TR, Harris CC. Frequent nitric oxide synthase-2 expression in human colon adenomas: implication for tumor angiogenesis and colon cancer progression. *Cancer Res* 1998;**58**: 334-41.

7. Cobbs CS, Brenman JE, Aldape KD, Bredt DS, Israel MA. Expression of nitric oxide synthase in human central nervous system tumors. *Cancer research* 1995;**55**: 727-30.

8. Eyler CE, Wu Q, Yan K, MacSwords JM, Chandler-Militello D, Misuraca KL, Lathia JD, Forrester MT, Lee J, Stamler JS, Goldman SA, Bredel M, et al. Glioma stem cell proliferation and tumor growth are promoted by nitric oxide synthase-2. *Cell* 2011;**146**: 53-66.

9. Cullis ER, Kalber TL, Ashton SE, Cartwright JE, Griffiths JR, Ryan AJ, Robinson SP. Tumour overexpression of inducible nitric oxide synthase (iNOS) increases angiogenesis and may modulate the anti-tumour effects of the vascular disrupting agent ZD6126. *Microvascular research* 2006;**71**: 76-84.

10. Jenkins DC, Charles IG, Thomsen LL, Moss DW, Holmes LS, Baylis SA, Rhodes P, Westmore K, Emson PC, Moncada S. Roles of nitric oxide in tumor growth. *Proceedings of the National Academy of Sciences of the United States of America* 1995;**92**: 4392-6.

11. Coulter JA, Page NL, Worthington J, Robson T, Hirst DG, McCarthy HO. Transcriptional regulation of inducible nitric oxide synthase gene therapy: targeting early stage and advanced prostate cancer. *The journal of gene medicine* 2010;**12**: 755-65.

12. Xie K, Huang S, Dong Z, Juang SH, Gutman M, Xie QW, Nathan C, Fidler IJ. Transfection with the inducible nitric oxide synthase gene suppresses tumorigenicity and abrogates metastasis by K-1735 murine melanoma cells. *J Exp Med* 1995;**181**: 1333-43.

13. Pipili-Synetos E, Papageorgiou A, Sakkoula E, Sotiropoulou G, Fotsis T, Karakiulakis G, Maragoudakis ME. Inhibition of angiogenesis, tumour growth and metastasis by the NO-releasing vasodilators, isosorbide mononitrate and dinitrate. *Br J Pharmacol* 1995;**116**: 1829-34.

14. Jadeski LC, Lala PK. Nitric oxide synthase inhibition by N(G)-nitro-L-arginine methyl ester inhibits tumor-induced angiogenesis in mammary tumors. *The American journal of pathology* 1999;**155**: 1381-90.

15. Konopka TE, Barker JE, Bamford TL, Guida E, Anderson RL, Stewart AG. Nitric oxide synthase II gene disruption: implications for tumor growth and vascular endothelial growth factor production. *Cancer Res* 2001;**61**: 3182-7.

16. Kamba T, McDonald DM. Mechanisms of adverse effects of anti-VEGF therapy for cancer. *Br J Cancer* 2007;**96**: 1788-95.

17. Malcolm GP, Jodrell DI, MacLellan A, Swaroop GR, Kelly PA, Whittle IR. Effects of nitric oxide manipulation on the disposition of platinum in an experimental glioma model. *Neuroreport* 1998;**9**: 181-5.

18. Gratton JP, Lin MI, Yu J, Weiss ED, Jiang ZL, Fairchild TA, Iwakiri Y, Groszmann R, Claffey KP, Cheng YC, Sessa WC. Selective inhibition of tumor microvascular permeability by cavtratin blocks tumor progression in mice. *Cancer cell* 2003;**4**: 31-9.

19. Ng QS, Goh V, Milner J, Stratford MR, Folkes LK, Tozer GM, Saunders MI, Hoskin PJ. Effect of nitric-oxide synthesis on tumour blood volume and vascular activity: a phase I study. *The lancet oncology* 2007;**8**: 111-8.

20. Ambs S, Merriam WG, Ogunfusika MO, Bennett WP, Ishibe N, Hussain SP, Tzeng EE, Geller DA, Billiar TR, Harris CC. p53 and vascular endothelial growth factor regulate tumor growth of NOS2-expressing human carcinoma cells. *Nature medicine* 1998;**4**: 1371-6.

21. Yamaguchi S, Bell HS, Shinoda J, Holmes MC, Wharton SB, Whittle IR. Glioma tumourgenicity is decreased by iNOS knockout: experimental studies using the C6 striatal implantation glioma model. *Br J Neurosurg* 2002;**16**: 567-72.

22. Kostourou V, Cartwright JE, Johnstone AP, Boult JK, Cullis ER, Whitley G, Robinson SP. The role of tumour-derived iNOS in tumour progression and angiogenesis. *Br J Cancer* 2011;**104**: 83-90.

23. Di Rosa M, Radomski M, Carnuccio R, Moncada S. Glucocorticoids inhibit the induction of nitric oxide synthase in macrophages. *Biochem Biophys Res Commun* 1990;**172**: 1246-52.

24. Miranda KM, Espey MG, Wink DA. A rapid, simple spectrophotometric method for simultaneous detection of nitrate and nitrite. *Nitric Oxide* 2001;**5**: 62-71.

25. Bradford MM. A rapid and sensitive method for the quantitation of microgram quantities of protein utilizing the principle of protein-dye binding. *Analytical biochemistry* 1976;**72**: 248-54.

26. Abramovitch R, Frenkiel D, Neeman M. Analysis of subcutaneous angiogenesis by gradient echo magnetic resonance imaging. *Magnetic resonance in medicine : official journal of the Society of Magnetic Resonance in Medicine / Society of Magnetic Resonance in Medicine* 1998;**39**: 813-24.

27. Howe FA, Robinson SP, McIntyre DJ, Stubbs M, Griffiths JR. Issues in flow and oxygenation dependent contrast (FLOOD) imaging of tumours. *NMR in biomedicine* 2001;**14**: 497-506.

28. Robinson SP, Rodrigues LM, Howe FA, Stubbs M, Griffiths JR. Effects of different levels of hypercapnic hyperoxia on tumour R(2)* and arterial blood gases. *Magnetic resonance imaging* 2001;**19**: 161-6.

29. Tropres I, Grimault S, Vaeth A, Grillon E, Julien C, Payen JF, Lamalle L, Decorps M. Vessel size imaging. *Magnetic resonance in medicine : official journal of the Society of Magnetic Resonance in Medicine / Society of Magnetic Resonance in Medicine* 2001;**45**: 397-408.

30. Schneider CA, Rasband WS, Eliceiri KW. NIH Image to ImageJ: 25 years of image analysis. *Nature methods* 2012;**9**: 671-5.

31. Vannini F, Kashfi K, Nath N. The dual role of iNOS in cancer. *Redox biology* 2015;**6**: 334-43.

32. Borutaite V, Budriunaite A, Brown GC. Reversal of nitric oxide-, peroxynitrite- and S-nitrosothiol-induced inhibition of mitochondrial respiration or complex I activity by light and thiols. *Biochimica et biophysica acta* 2000;**1459**: 405-12.

33. Lee DH, Pfeifer GP. Mutagenesis induced by the nitric oxide donor sodium nitroprusside in mouse cells. *Mutagenesis* 2007;**22**: 63-7.

34. Jordan BF, Misson P, Demeure R, Baudelet C, Beghein N, Gallez B. Changes in tumor oxygenation/perfusion induced by the no donor, isosorbide dinitrate, in comparison with carbogen: monitoring by EPR and MRI. *International journal of radiation oncology, biology, physics* 2000;**48**: 565-70.

35. Oronsky BT, Scicinski JJ, Reid T, Knox S. Beyond antiangiogenesis: vascular modulation as an anticancer therapy-a review. *Translational oncology* 2012;**5**: 133-40.

36. Gossen M, Bujard H. Tight control of gene expression in mammalian cells by tetracycline-responsive promoters. *Proceedings of the National Academy of Sciences of the United States of America* 1992;**89**: 5547-51.

37. Senner V, Sturm A, Hoess N, Wassmann H, Paulus W. In vivo glioma model enabling regulated gene expression. *Acta neuropathologica* 2000;**99**: 603-8.

38. Swaroop GR, Kelly PA, Bell HS, Shinoda J, Yamaguchi S, Whittle IR. The effects of chronic nitric oxide synthase suppression on glioma pathophysiology. *British journal of neurosurgery* 2000;**14**: 543-8.

39. Jadeski LC, Hum KO, Chakraborty C, Lala PK. Nitric oxide promotes murine mammary tumour growth and metastasis by stimulating tumour cell migration, invasiveness and angiogenesis. *International journal of cancer Journal international du cancer* 2000;**86**: 30-9.

40. Whittle IR, Collins F, Kelly PA, Ritchie I, Ironside JW. Nitric oxide synthase is expressed in experimental malignant glioma and influences tumour blood flow. *Acta neurochirurgica* 1996;**138**: 870-5; discussion 5-6.

41. Swaroop GR, Malcolm GP, Kelly PA, Ritchie I, Whittle IR. Effects of nitric oxide modulation on tumour blood flow and microvascular permeability in C6 glioma. *Neuroreport* 1998;**9**: 2577-81.

42. Howe FA, McPhail LD, Griffiths JR, McIntyre DJ, Robinson SP. Vessel size index magnetic resonance imaging to monitor the effect of antivascular treatment in a rodent tumor model. *Int J Radiat Oncol Biol Phys* 2008;**71**: 1470-6.

43. Abramovitch R, Dafni H, Smouha E, Benjamin LE, Neeman M. In vivo prediction of vascular susceptibility to vascular susceptibility endothelial growth factor withdrawal: magnetic resonance imaging of C6 rat glioma in nude mice. *Cancer research* 1999;**59**: 5012-6.

44. Burrell JS, Walker-Samuel S, Baker LC, Boult JK, Jamin Y, Ryan AJ, Waterton JC, Halliday J, Robinson SP. Evaluation of novel combined carbogen USPIO (CUSPIO) imaging biomarkers in assessing the antiangiogenic effects of cediranib (AZD2171) in rat C6 gliomas. *International journal of cancer Journal international du cancer* 2012;**131**: 1854-62.

45. Burrell JS, Walker-Samuel S, Baker LC, Boult JK, Ryan AJ, Waterton JC, Halliday J, Robinson SP. Investigating temporal fluctuations in tumor vasculature with combined carbogen and ultrasmall superparamagnetic iron oxide particle (CUSPIO) imaging. *Magnetic resonance in medicine : official journal of the Society of Magnetic Resonance in Medicine / Society of Magnetic Resonance in Medicine* 2011;**66**: 227-34.

46. Kashiwagi S, Izumi Y, Gohongi T, Demou ZN, Xu L, Huang PL, Buerk DG, Munn LL, Jain RK, Fukumura D. NO mediates mural cell recruitment and vessel morphogenesis in murine melanomas and tissue-engineered blood vessels. *The Journal of clinical investigation* 2005;**115**: 1816-27.

47. Yu J, deMuinck ED, Zhuang Z, Drinane M, Kauser K, Rubanyi GM, Qian HS, Murata T, Escalante B, Sessa WC. Endothelial nitric oxide synthase is critical for ischemic remodeling, mural cell recruitment, and blood flow reserve. *Proceedings of the National Academy of Sciences of the United States of America* 2005;**102**: 10999-1004.

Figure legends

Figure 1 *In vitro* characterization of C6 pTet-off asiNOS cells in the presence and absence of doxycycline.

Cells were treated for 4 days with 2 µg/ml doxycycline. For the last 2 days, cells were also stimulated with cytokines (10 ng/ml TNF-α, 1000 U/ml IFN-γ) and 5 µg/ml LPS. **A:** iNOS (131 kDa) expression determined by western blot. The integrated density of the individual bands for iNOS was corrected using α-actin (42 kDa). Results are mean +1 SEM of three separate experiments (***P* < 0.01). **B:** Nitrite production. Results are the mean +1 SEM of three separate experiments performed in triplicate (****P* < 0.001).

Figure 2 *In vivo* characterization of control and doxycycline treated C6 pTet-off asiNOS xenografts.

Cells (2 x 10^6) were injected into the flanks of nude mice. Mice were given 0.2 mg/ml doxycycline in 5% (w/v) sucrose (+dox, *n* = 5) or 5% (w/v) sucrose alone (-dox, *n* = 4) in the drinking water *ad libitum*. **A:** Western blot of tumour homogenates and the mean box plot distributions of the integrated densities of the individual bands for iNOS corrected using α-actin, showing that doxycycline regulates iNOS expression (**P* < 0.05). **B:** NOx production by tumours determined in homogenates. Results are the mean +1 SEM of triplicate measurements made from all tumours in each group (**P* < 0.05, Unpaired t-test on the transformed data (Y=Log(Y)). **Note:** Logarithmic transformation was used to normalize the skewed data. C: Mean tumour growth curves for C6 iNOS-inducible NO^- (*n* = 6) and NO^+ (*n* = 5) tumours, showing that reduced iNOS expression delays tumour growth (day 46: **P* < 0.05).

Figure 3 Effects of NO down-regulation on tumour vascular development as determined by MRI of C6 pTet-off asiNOS xenografts.

A: Representative T_2-weighted images, parametric maps of baseline $R_2^*_{air}$, fractional blood volume (fBV) and $\Delta R_2^*_{CB}$ in response to carbogen, from the central tumour slice. ROIs

encompassing the whole tumour volume are demarcated on the T_2-weighted images. **B,C,D:** Box plot distributions of the median fBV values measured over the whole tumour volume **(B)**, and the median fBV values **(C)** and the median $\Delta R_2^*{}_{CB}$ values **(D)** in regions where fBV is higher than the median fBV value of all the data, of NO^- (*n* = 4) or NO^+ (*n* = 5) tumours (**P* < 0.05).

Figure 4 Histological assessment of the vasculature of C6 pTet-off asiNOS xenografts in the absence or presence of doxycycline.

A: RGB images are composite images from frozen whole tumour sections stained with the perfusion marker Hoechst 33342 and the hypoxia marker pimonidazole. Hoechst 33342 perfused tumour blood vessels fluoresce blue, and areas of pimonidazole adducts fluoresce green. **B:** H&E-stained sections indicating necrotic regions (arrows). **C:** RGB images are composite images from frozen sections stained with the endothelial cell marker CD31, detected using a biotinylated goat anti-rat IgG attached to Fluorescein Avidin D that fluoresces green, and the perivascular cell marker α-SMA, detected using an Alexa-546-conjugated secondary antibody that fluoresces red. Scale bar is 1 mm.

Figure 5 Quantification of histological markers of tumour vasculature for C6 pTet-off asiNOS xenografts.

A: Hoechst 33342 perfused area, **B:** Pimonidazole adduct area, **C:** Necrotic area, **D:** Endothelial cell content (CD31 stained area), **E:** Perivascular cell coverage (α-SMA stained area), and **F:** fraction of mature vessels (α-SMA/CD31 ratio) of C6 iNOS-inducible NO^- and NO^+ tumours. Results are means +1 SEM of three sections per tumour for *n* = 4 in the NO^- and *n* = 5 in the NO^+ group (**P* < 0.05, ***P* < 0.01).

Figure 6 Investigation of the effect of NO synthesis on VEGF expression *in vitro* and *in vivo.*

A: VEGF production in conditioned medium from C6 pTet-off asiNOS cells treated with 2μg/ml doxycycline for 5 days. For the last 3 days, cells were also stimulated with cytokines (10 ng/ml TNF-α, 1000 U/ml IFN-γ) and 5 μg/ml LPS. Results are means + 1 SEM of three separate experiments in duplicate (*$P < 0.05$, **$P < 0.01$). **B:** VEGF expression in C6 iNOS-inducible tumour homogenates. Tumours derived from animals provided with drinking water containing 0.2 mg/ml doxycycline in 5% (w/v) sucrose (NO^+, $n = 4$) or 5% (w/v) sucrose alone (NO^-, $n = 5$). Results are means +1 SEM of triplicate measurements made from all tumours in each group.

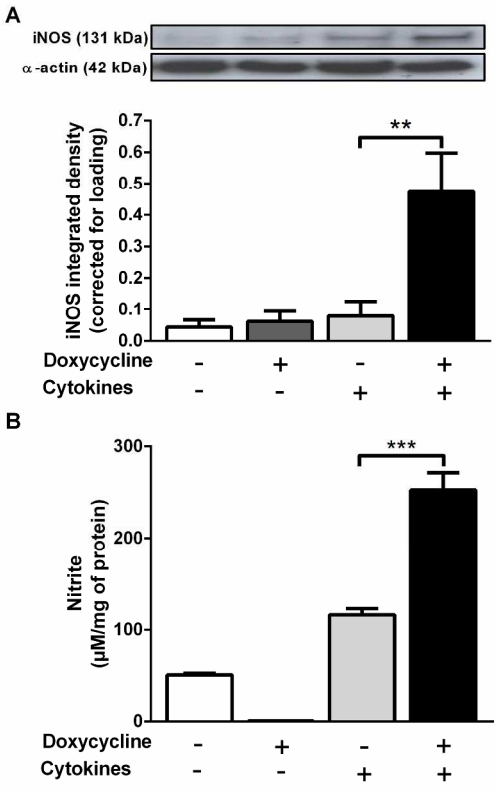

In vitro* characterization of C6 pTet-off asiNOS cells in the presence and absence of doxycycline.** Cells were treated for 4 days with 2 µg/ml doxycycline. For the last 2 days, cells were also stimulated with cytokines (10 ng/ml TNF-α, 1000 U/ml IFN-γ) and 5 µg/ml LPS. **A:** iNOS (131 kDa) expression determined by western blot. The integrated density of the individual bands for iNOS was corrected using α-actin (42 kDa). Results are mean +1 SEM of three separate experiments (**$P < 0.01$). **B:** Nitrite production. Results are the mean +1 SEM of three separate experiments performed in triplicate ($P < 0.001$).

268x396mm (300 x 300 DPI)

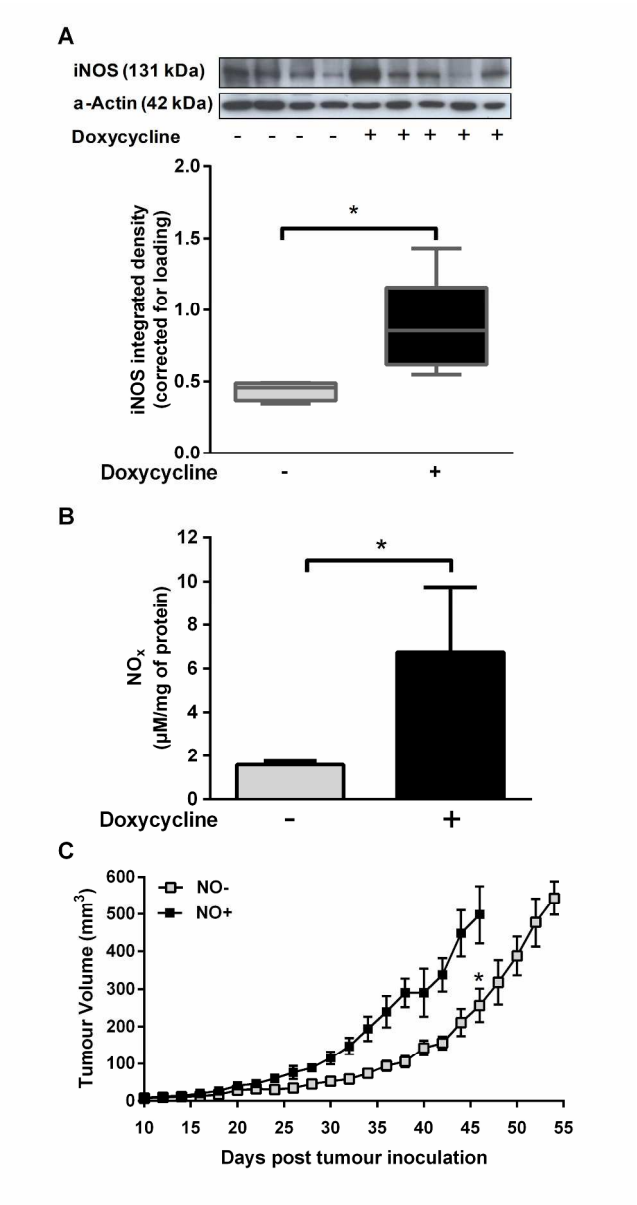

***In vivo* characterization of control and doxycycline treated C6 pTet-off asiNOS xenografts.** Cells (2 x 10^6) were injected into the flanks of nude mice. Mice were given 0.2 mg/ml doxycycline in 5% (w/v) sucrose (+dox, *n* = 5) or 5% (w/v) sucrose alone (-dox, *n* = 4) in the drinking water *ad libitum*. **A:** Western blot of tumour homogenates and the mean box plot distributions of the integrated densities of the individual bands for iNOS corrected using α-actin, showing that doxycycline regulates iNOS expression (**P* < 0.05). **B:** NOx production by tumours determined in homogenates. Results are the mean +1 SEM of triplicate measurements made from all tumours in each group (**P* < 0.05, Unpaired t-test on the transformed data (Y=Log(Y)). **Note:** Logarithmic transformation was used to normalize the skewed data. **C:** Mean tumour growth curves for C6 iNOS-inducible NO- (*n* = 6) and NO+ (*n* = 5) tumours, showing that reduced iNOS expression delays tumour growth (day 46: **P* < 0.05).

217x410mm (300 x 300 DPI)

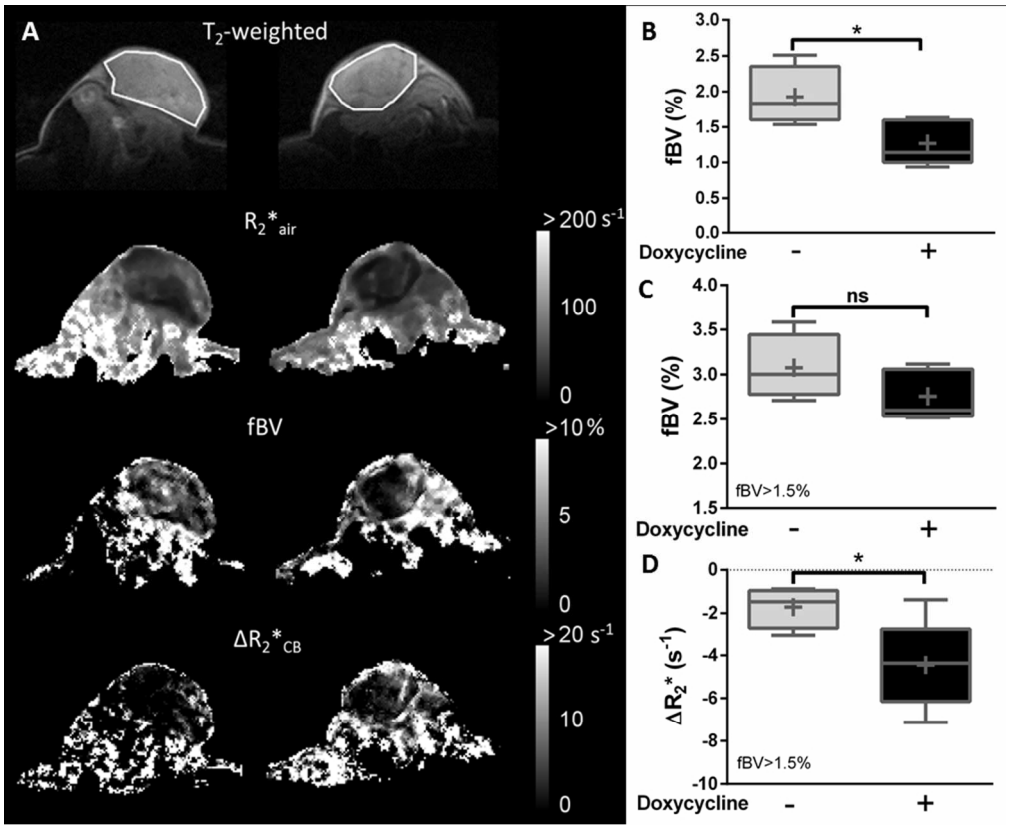

Effects of NO down-regulation on tumour vascular development as determined by MRI of C6 pTet-off asiNOS xenografts.

A: Representative T_2-weighted images, parametric maps of baseline $R_2{}^*_{air}$, fractional blood volume (fBV) and $\Delta R_2{}^*_{CB}$ in response to carbogen, from the central tumour slice. ROIs encompassing the whole tumour volume are demarcated on the T_2-weighted images. **B,C,D:** Box plot distributions of the median fBV values measured over the whole tumour volume **(B)**, and the median fBV values **(C)** and the median $\Delta R_2{}^*_{CB}$ values **(D)** in regions where fBV is higher than the median fBV value of all the data, of NO^- (n = 4) or NO^+ (n = 5) tumours (*P < 0.05).

169x138mm (150 x 150 DPI)

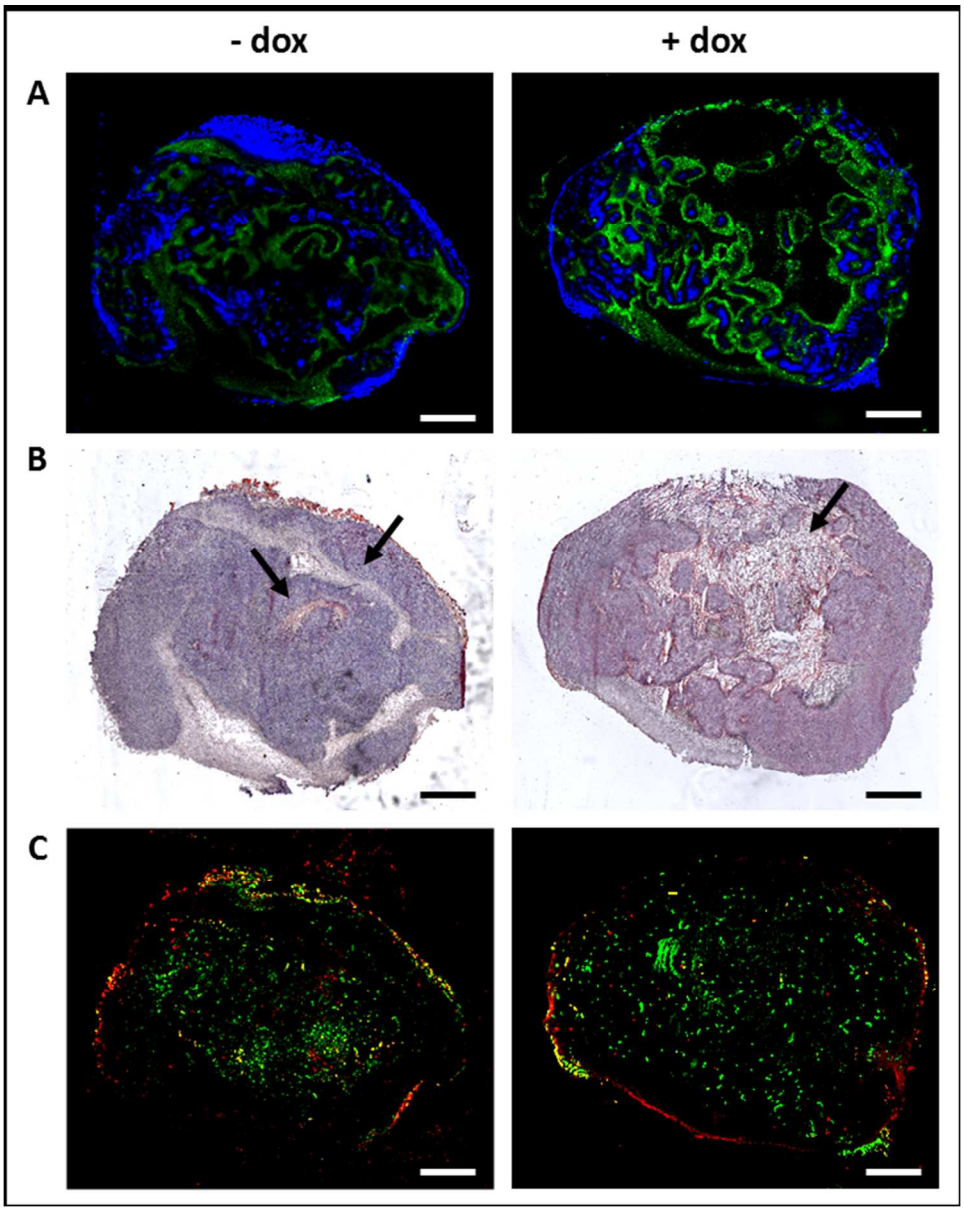

Histological assessment of the vasculature of C6 pTet-off asiNOS xenografts in the absence or presence of doxycycline.

A: RGB images are composite images from frozen whole tumour sections stained with the perfusion marker Hoechst 33342 and the hypoxia marker pimonidazole. Hoechst 33342 perfused tumour blood vessels fluoresce blue, and areas of pimonidazole adducts fluoresce green. **B:** H&E-stained sections indicating necrotic regions (arrows). **C:**RGB images are composite images from frozen sections stained with the endothelial cell marker CD31, detected using a biotinylated goat anti-rat IgG attached to Fluorescein Avidin D that fluoresces green, and the perivascular cell marker α-SMA, detected using an Alexa-546-conjugated secondary antibody that fluoresces red. Scale bar is 1 mm.

123x154mm (150 x 150 DPI)

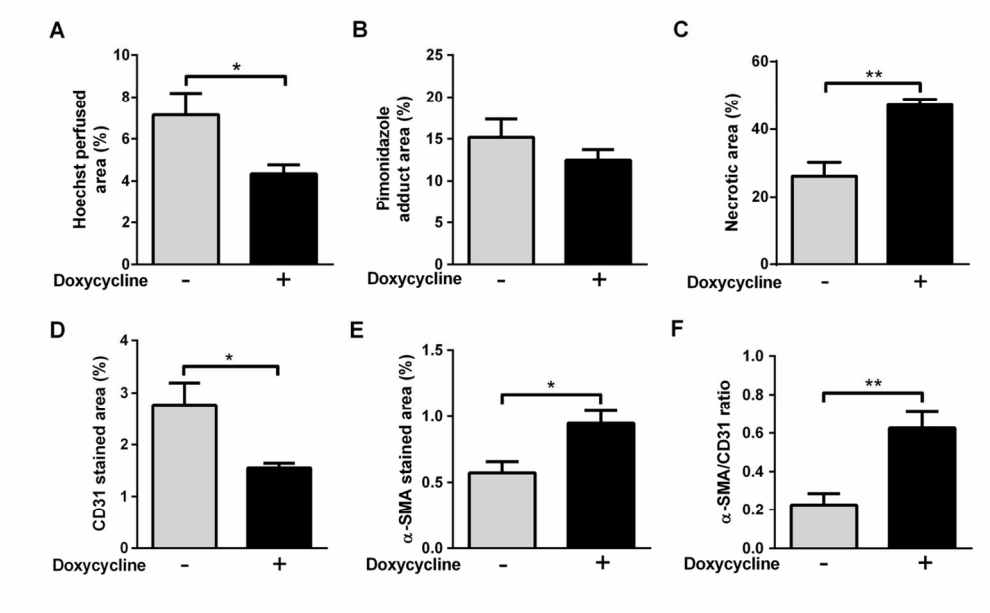

Quantification of histological markers of tumour vasculature for C6 pTet-off asiNOS xenografts. **A:** Hoechst 33342 perfused area, **B:** Pimonidazole adduct area, **C:** Necrotic area, **D:** Endothelial cell content (CD31 stained area), **E:** Perivascular cell coverage (α-SMA stained area), and **F:** fraction of mature vessels (α-SMA/CD31 ratio) of C6 iNOS-inducible NO^- and NO^+ tumours. Results are means +1 SEM of three sections per tumour for n = 4 in the NO^- and ^{n} = 5 in the NO^+ group (*P < 0.05, **P < 0.01).

116x71mm (300 x 300 DPI)

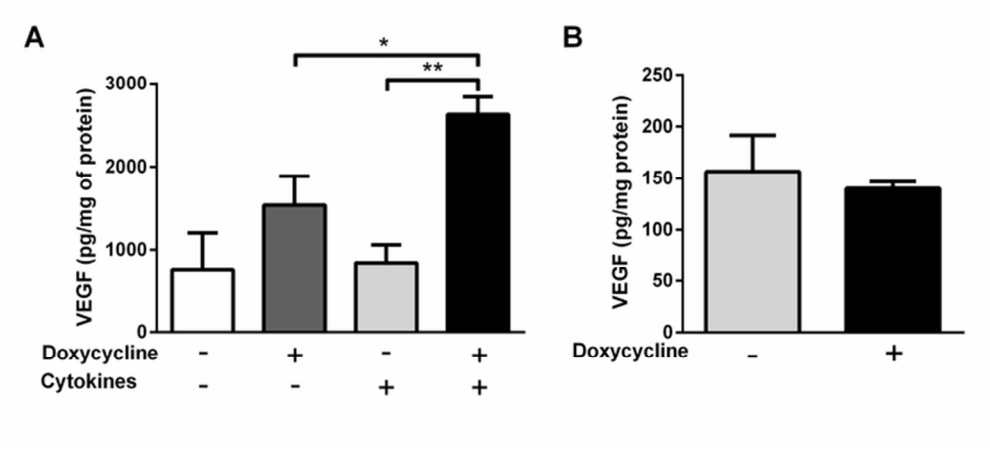

Investigation of the effect of NO synthesis on VEGF expression *in vitro* and *in vivo*.
A: VEGF production in conditioned medium from C6 pTet-off asiNOS cells treated with 2µg/ml doxycycline for 5 days. For the last 3 days, cells were also stimulated with cytokines (10 ng/ml TNF-α, 1000 U/ml IFN-γ) and 5 µg/ml LPS. Results are means + 1 SEM of three separate experiments in duplicate (*$P < 0.05$, **$P < 0.01$). **B:** VEGF expression in C6 iNOS-inducible tumour homogenates. Tumours derived from animals provided with drinking water containing 0.2 mg/ml doxycycline in 5% (w/v) sucrose (NO^+, $n = 4$) or 5% (w/v) sucrose alone (NO^-, $n = 5$). Results are means +1 SEM of triplicate measurements made from all tumours in each group.
65x29mm (300 x 300 DPI)